



SHAPE DISTORTIONS, PLASTIC DEFORMATIONS AND RESIDUAL STRESSES AFTER ONE-SIDED FORGING/ROLLING OF THE BEAM: THE CASE OF ADDITIVE MANUFACTURING OF THE LINEAR METAL SEGMENT WITH LAYER-BY-LAYER PRESSURE TREATMENT

I.E. Keller^{1,2}, A.V. Kazantsev², D.S. Dudin^{1,2}, G.L. Permyakov², M.F. Kartashev²

¹*Institute of Continuous Media Mechanics, Ural branch, Russian Academy of Sciences, Perm, Russian Federation*

²*Perm National Research Polytechnic University, Perm, Russian Federation*

The paper aims at constructing a numerical model of the stress-strain state in a prismatic beam under one-sided plastic deformation. This model provides a range of optimal modes of the layer-by-layer pressure treatment of additively manufactured linear metal segments. Shape distortions, residual stresses and strength characteristics can be controlled through forging or rolling of the deposited metal layers. We model the process consisting of a stage of the one-sided surface pressure treatment of the sample clamped to the opposite face of a flat surface by normal couplings, and a stage of releasing the sample from the clamps. According to the experimental data, the impact of a pneumatic hammer is calibrated in the numerical model and the equivalent depth of the roller insertion is determined. We investigate the distribution inhomogeneity of plastic deformations and longitudinal residual stresses along the cross-section of the sample, the longitudinal and transverse curvature of the latter, the nature of deformations during the sample unloading for AMg6 and VT6 alloys and 12X18N10T stainless steel depending on the depth of the roller insertion. For each of the materials, the critical roller insertion depth is found, after which the sign of the longitudinal curvature of the sample changes. The anticlastic curvature of the samples of sufficiently large widths was found. We discuss the experimental methods of finding the state of the clamped sample (a part of the linear metal segment) based on its unloaded state. The acceptability of measurements of microhardness distribution is outlined over the height of the cross-section of the sample to estimate the localization zone size of plastic deformations, as well as the acceptability of measurements of the longitudinal curvature of the sample for estimations of residual stresses. It has been shown not to be advisable to measure the longitudinal residual stresses due to their significant heterogeneity, as well as redistribution during cutting layers.

Key words: additive manufacturing, layer-by-layer forging, localization of plastic deformations, residual stresses, numerical calculation, experiment

1. Problem and research target

Wire-arc additive manufacturing makes it possible to create metal products of complex shapes with significant material savings. This technology synthesizes an almost continuous metal; however, its dendritic structure does not provide the strength characteristics of a rolled metal. As part of research collaborations and projects, to obtain a homogeneous grain structure of the material, some universities (Cranfield and Manchester Universities [1–6], Indian Institute of Technology Bombay [7–8], Perm National Research Polytechnic University [9–12]) use hybrid technologies to manufacture large segmented products with a sequential deposition of layers followed by forging or rolling.

By controlling the modes of deposition and forging/rolling during hybrid additive manufacturing, it is possible to obtain a homogeneous fine-grained structure due to recrystallization or phase transformations occurring in the work-hardened metal at high temperatures. Apart from improving the entire range of strength characteristics, these modes serve well to correct the field of residual stresses and distortions of the structure geometry caused by them. Eigen deformations caused by crystallization and cooling of the deposited layer, as well as plastic deformation of workpieces, generate residual stresses that can relax due to grain transformations. To control these processes, it is necessary to build a coupled model of solid mechanics and understand particular problems.

The work focuses on shape distortions, localization of plastic deformations and distribution of residual stresses caused by one-sided forging or rolling of the beam. These phenomena will be investigated for alloys AMg6, VT6 and stainless steel 12Kh18N10T with numerical calculations of the model problems of one-sided forging and rolling of the beam using LS-DYNA[®] software package and comparing the calculated data with the experimental results, which have been found by measuring

the bending and distributions of microhardness and residual stresses in the sections of the workpiece subjected to one-sided forging with a pneumatic hammer.

The obtained results are used to select optimal modes of the pressure treatment of the deposited layer, which provides the necessary work hardening of the metal, transforms dendrites into a fine-grained crystalline structure at critical temperatures accompanying the deposition of the following layers. In each of the considered metal alloys, different mechanisms of grain structure transformation (recrystallization in the aluminum alloy, martensitic transformations in austenitic stainless steel and titanium alloy) are established but they occur according to the general scenario (hardening with a subsequent exposure to temperature). Therefore, the selected problem and the corresponding mathematical model are important to set up the technology of additive manufacturing of products from a wide range of structural metal alloys. Strain hardening and recrystallization in a solid have little effect on thermophysical processes in the deposited material. It is possible to formulate an uncoupled model where the problem of crystallization, heat and mass transfer are solved separately. As a result, we find the distribution of temperatures in the workpiece and eigen deformations of the shrinkage in the attached layer. In this approach, the main problem lies in the transformation of the material grain structure in the known fields of residual stresses caused by incompatible shrinkage and plastic deformations. The problem considered below is important to evaluate the contribution of the pressure treatment to the stress-strain state of the workpiece.

2. Statement of the model problem and numerical solution

There is a straight prismatic beam with a rectangular section, which we consider to be an idealized linear element (linear metal segment) of the deposited segmented structure. The lower face of the beam is rigidly clamped along the normal to it, and there is no limit on small deformations in the plane of this face. These limitations most accurately reflect the experiment organized to confirm the results of solving the model problem, which will be discussed in the next section. The upper face of the beam is subjected to forging or rolling, i.e. a *spot* pressure treatment technology that ensures the localization of plastic deformation near the treated surface (Fig. 1).

It is known [13–18] that the longitudinal plastic bending of the beam is sensitive to ratio h/b , where h is height, b is width of a rectangular cross-section, the variation of which from 0 to ∞ corresponds to a change in the scheme from the plane deformed to the plane stress state in the transverse direction. Depending on this parameter, there come changes of the distribution over the cross-section of the longitudinal component of residual stresses, the longitudinal and transverse curvatures of the beam and boundary effects. To apply the results to stackable linear elements with various cross-sectional form factors, the model problem is solved for bodies with several values of. If $h/b \rightarrow 0$, when the beam turns into a plate, the loading scheme considered here is different from the loading scheme for the shot blasting of the plate [19], which will be discussed in the analysis of the results.

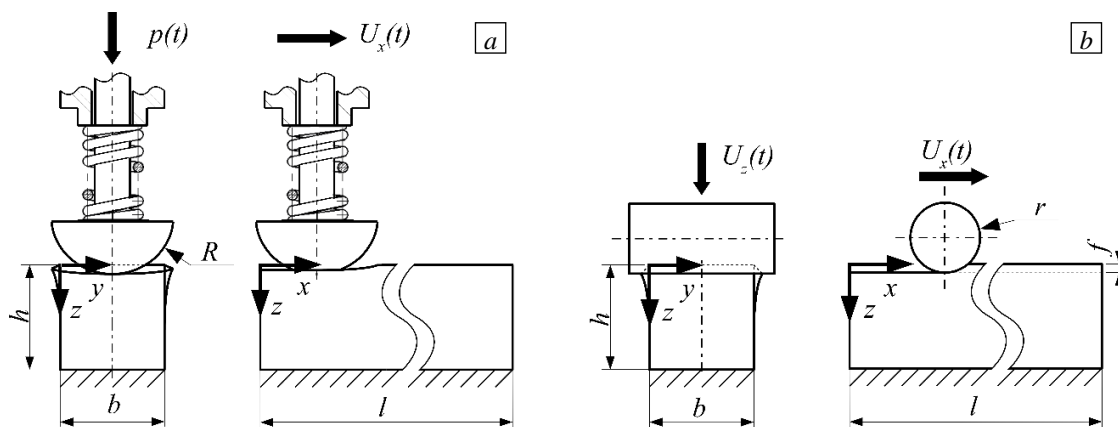


Fig. 1. Computational schemes of forging (a) and rolling (b) of the sample.

The loading is organized in two steps: 1) a one-side forging or rolling using the fixed workpiece; 2) releasing the workpiece from the clamps. The 1st stage corresponds to forging of the linear metal segment; the 2nd stage makes it possible to compare the deflection of the beam and the distributions of residual stresses and strain working over its sections with the experiment. Both stages are calculated in the elastoplastic formulation.

To describe large plastic and small elastic deformations of metals, the standard model [20, 21] is used in terms of the current Lagrangian approach in rate statement, numerically implemented in package LS-DYNA[®]. The additivity of elastic and strain-rate tensors is accepted, while the elastic tensor is linearly related to the Jaumann derivative of the Kirchhoff stress tensor, and the strain-rate tensor is related to the law of plastic flow

$$d_{ij}^p = \frac{1}{H} \dot{s}_{ij} \frac{s_{ij}}{\sigma_u}, \quad (1)$$

where d_{ij}^p are components of deviator of strain-rate tensor, $s_{ij} = \sigma_{ij} - \sigma_{kk} \delta_{ij}$ are components of stress deviator, \dot{s}_{ij} is the material derivative of this tensor, σ_u is the yield stress under uniaxial stretching, H is parameter of strain hardening $H = \partial \sigma_u / \partial \varepsilon_p$. (1) implies the plastic potential associated with the von Mises yield criterion

$$\sigma_M = \sigma_u. \quad (2)$$

In this case, $\sigma_M = \sqrt{3s_{ij}s_{ij}/2}$ is the stress intensity, and for the yield strength σ_u under uniaxial tension, the Johnson–Cook isotropic hardening law is adopted in the following form:

$$\sigma_u = \left(A + B \varepsilon_p^n \right) \left(1 + C \ln \frac{\dot{\varepsilon}_p}{\dot{\varepsilon}_*} \right), \quad (3)$$

where $\dot{\varepsilon}_p = \sqrt{2d_{ij}^p d_{ij}^p / 3}$ is the intensity of strain rates, $\varepsilon_p = \int_0^t \dot{\varepsilon}_p dt$ are the accumulated plastic deformations. Parameter H in (1) is found from law (3). In the LS-DYNA[®] package, this model corresponds to the standard material MAT_098 [21]. The dependence on the strain rate was taken into account for AMg6 material, for which, in the numerical model of forging, the effect of an air hammer was calibrated and the equivalent indentation depth of the tool was determined in the calculation in case of rolling.

Constants A , B , C , $\dot{\varepsilon}_*$, n of the Johnson–Cook isotropic hardening law are taken (or obtained after the data approximation) from [22] for Amg6, from [23] for 12X18H10T and from [24] for VT6. The numerical data are given in Table 1.

Table 1. Constants of the Johnson–Cook hardening law.

Material	A , MPa	B , MPa	C	$\dot{\varepsilon}_*$, s ⁻¹	n
AMg6	184	4210	0.0474	1	1.2
12X18H10T	305	1161	0	1	0.61
VT6	968	380	0	1	0.42

The numerical solution of the contact dynamic problem of plastic deformations of the beam in a quasi-static formulation was performed in the LS-DYNA[®] package, which implements the finite element method taking into account geometric and elastic-plastic nonlinearities. When solving

problems of pressure treatment, the integration of the equations of motion of an ensemble of finite elements with more than 100 thousand degrees of freedom was performed using an explicit scheme. The stage of releasing the beam from the clamps was considered in an elastic-plastic formulation based on an implicit scheme. In the implicit integration scheme, 8-node elements with integration of the strain field at eight Gauss points were used, in the explicit scheme, 8-node elements with a single integration point were used. The algorithm of solving the contact problem assumed assigning the sets consisting of nodes and faces of the elements of the contacting surfaces. The correct operation of the contact group was achieved by selecting the coefficient of contact stiffness. The coefficient of dry friction was assumed to be zero. The initial density and elastic constants are listed in Table 2.

Table 2. Physical constants of materials.

Material	ρ_0 , kg/m ³	E , GPa	ν
AMg6	2640	71	0.3
VT6	4450	115	0.32
12X18H10T	7800	206	0.3

The explicit scheme with the time step, according to the Courant criterion, is directly proportional to the square root of the density of the material, required a reduction in the computation time, typical for problems solved within quasistatics. To do this, the density of the workpiece material was artificially increased, and the emerging dynamic effects were eliminated by selecting acceptable coefficients of dissipation of the kinetic energy of the system. The taken measures correspond to the recommendations of software developers [25, 26].

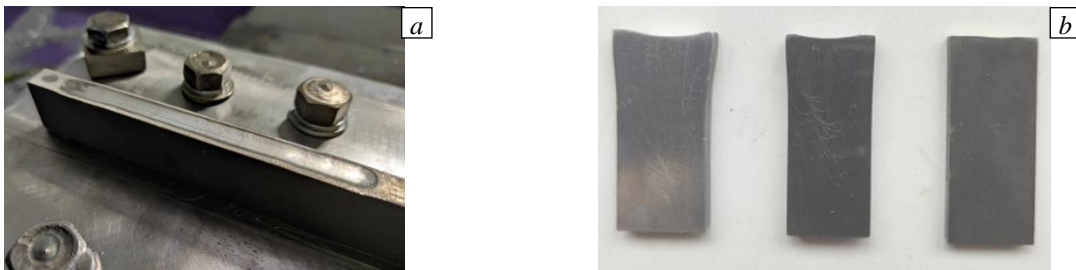


Fig. 2. Forged sample (a) and distorted cross-sections of samples from materials AMg6, 12X18H10T and VT6 (b).

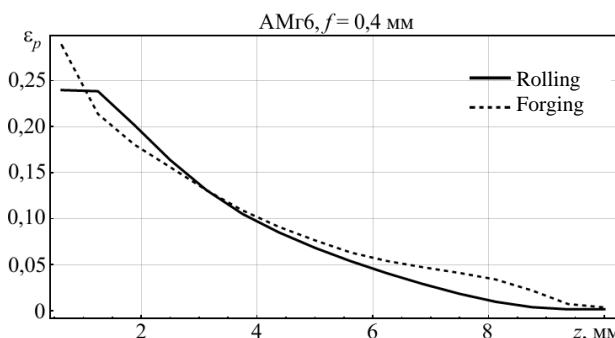


Fig. 3. Distribution of accumulated plastic deformations over the height of the sample cross-section along the plane of symmetry.

products, annealed at a temperature of 550°C for 3 hours and cooled in air, was pressed at the ends against a hard surface and forged from the narrow side. The distortions of its cross-section in four cuts were measured using Hirox KH-7700 digital optical microscope. They were localized at a depth of 7–9 mm from the rolled surface (Fig. 2). The calibration of tension in the numerical calculation is carried out along the longitudinal and transverse deformations of the section in the area of

The impact parameters during forging with an air hammer had the following values: impact energy was 19.74 J; frequency was 2820 beats/min; working pressure was 0.63 MPa; striker pressure was 0.2 MPa; the speed of movement of the striker along the workpiece was 300 mm/min. The striker had a spherical tip with a radius of $R = 15$ mm. The power of impact in the numerical model was calibrated using the following experiment. A bar with dimensions of 250×24×10 mm made of AMg6 rolled

deformation localization (Fig. 3). Since it takes 4 times longer to calculate forging operations of a beam compared to rolling operations, and also due to the fact that rolling results in a greater uniformity of distribution of stresses and deformations along the transverse coordinate, most of the numerical results in this study are obtained for the problem of rolling (with the roller radius of $r = 7.5$ mm). In this problem, the values of plastic strains and the depth of their localization, comparable with those observed during forging, corresponded to the penetration depth of the roller $f = 0.4$ mm (Fig. 3).

3. Distribution of stresses and deformations

A beam with a length of $l = 200$ mm clamped to a rigid horizontal surface with normal couplings along one side, was rolled along a parallel side and released from the clamps. For all materials under consideration, the longitudinal curvature, distributions of plastic deformations and residual stresses over the cross section are studied depending on the depth of rolling and the shape of the cross-section.

Figure 4 shows the distributions of the longitudinal component of residual stresses and accumulated plastic deformations over the cross-section of the sample from AMg6 corresponding to the middle of the sample length. It can be seen that the distributions are inhomogeneous along the transverse coordinate. In addition, the equilibrium, which requires that the total value σ_x of the cross-section is equal to zero, is not satisfied along any segment along the coordinate, which makes it difficult to control the data in the experimental investigations of residual stresses. Nevertheless, further field distributions will be studied along the segment lying on the axis of the symmetry of the cross-section.

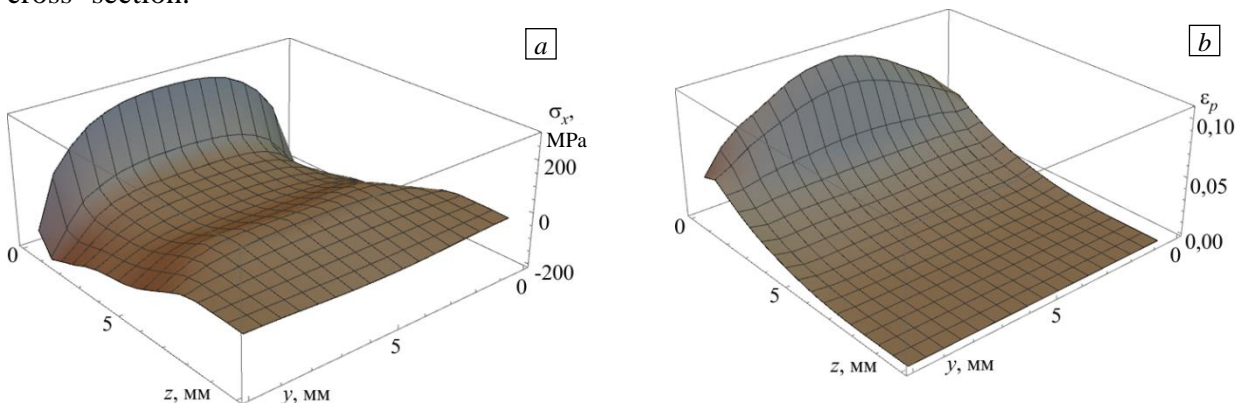


Fig. 4. Distributions of longitudinal residual stresses (a) and accumulated plastic deformations (b) along the transverse cross-section in the middle of the sample from AMg6 when $f = 0,1$ mm.

Figure 5 shows the distributions of the longitudinal component of residual stresses and the transverse component of plastic deformations along the segment indicated above depending on the depth of rolling. It can be seen that for all the materials under study, the longitudinal stress component

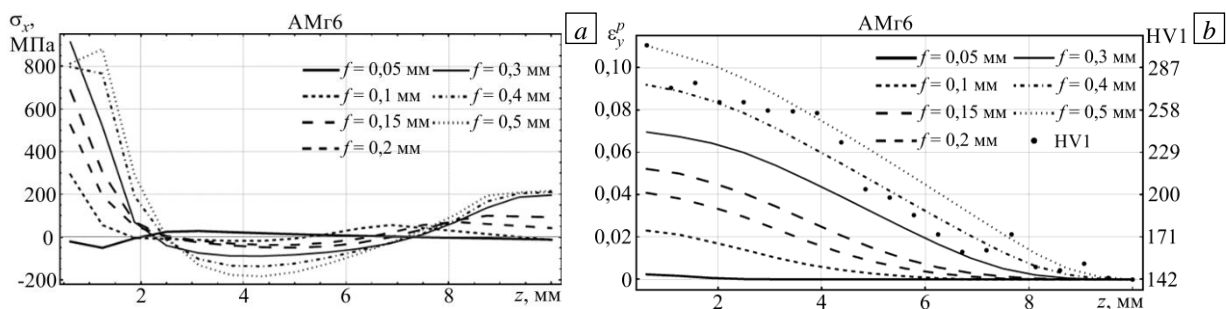


Fig. 5. Distributions of longitudinal residual stresses (a), transverse plastic deformations and microhardness (b) along the height of the samples made from different materials at different depths of the roller insertion.

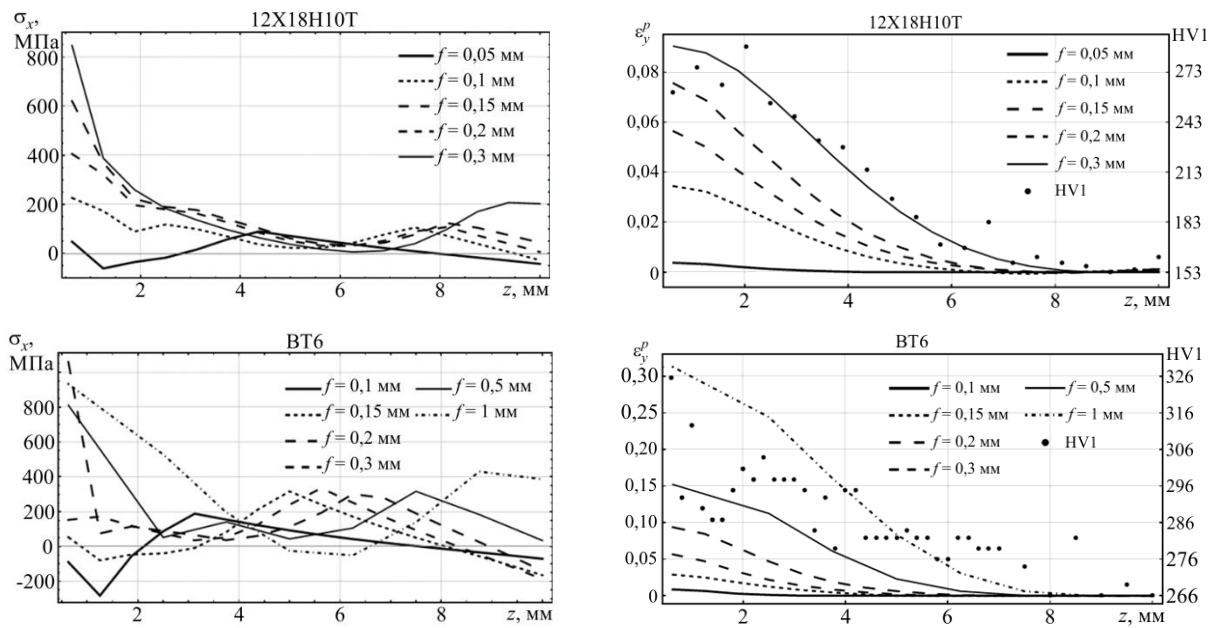


Fig. 5. Continuation.

is not in equilibrium along this segment in the integral sense. It turned out that the distributions of the transverse component of plastic deformations are almost congruent to the distributions of accumulated plastic deformations and are given here for a subsequent comparison with the values of the longitudinal component. The graphs show the growth of the plastic zone with an increase in the rolling depth (here HV1 is microhardness). Let us consider that the rolling depths equivalent to the action of an air hammer are 0.4 mm for AMg6, 0.2 mm for 12X18H10T and 0.1 mm for VT6. The increased maximum stresses in the calculations are explained with the imperfection of the approximation of hardening curves based on the Johnson–Cook law.

For comparison, Figure 6 shows the curves of the total and plastic longitudinal deformations before (ϵ_x^0 and ϵ_x^{p0}) and after (ϵ_x and ϵ_x^p) the release of the sample from the clamps. The diagrams of both parameters indicate the elastic nature of the deformation of the sample after its release, which is recorded for samples from AMg6 and 12Kh18N10T for all degrees of rolling and for a sample from VT6 it is $f = 0.1 \div 0.2$ mm. The unloading [a]mples from VT6 (rolled more than 0.3 mm [b]p) is accompanied by plastic shear. Figure 6 also shows that the gradients of total longitudinal deformations corresponding to the rolling depths of 0.05 and 0.4 mm have different signs, which also indicates different signs of the curvatures of the unloaded samples.

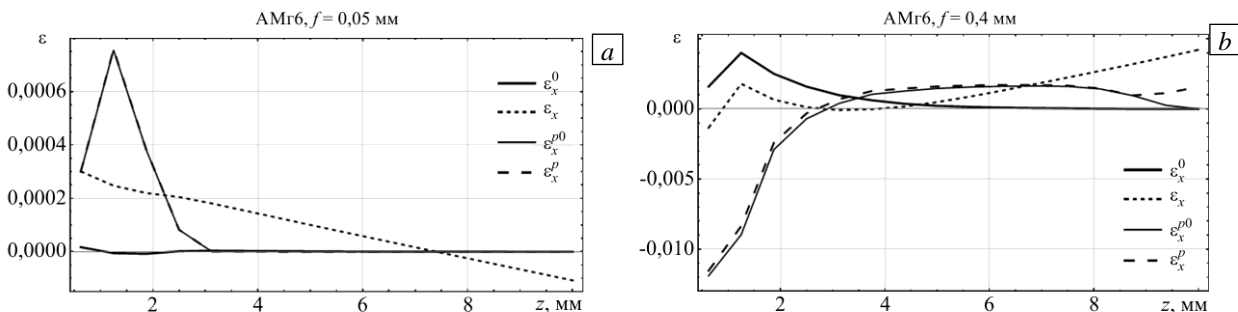


Fig. 6. Distributions of longitudinal total and plastic deformations over the cross-section of the sample from AMg6 in the case of clamping (a) and after releasing (b).

To study the longitudinal bending of the unloaded samples, depending on the depth of rolling, their curvatures are determined at three points of the surface lamped during the rolling (at 25, 50 and 75 % of the sample length l). Figure 7a indicates the presence of successive phases of growth, decrease,

and sign change in the curves with an increase in the degree of surface deformations. At small depths of rolling, the sample has a buckling facing the tool, while at large depths it is directed away from it. This fact was previously noted in [18] for plates subjected to one-sided shot peening. In contrast to the loading schemes considered in [13–17], here the bending is caused by a longitudinal moment uniformly distributed along the length of the bar, which arises due to an incompatible plastic deformation field. This is mainly responsible for the transverse components of plastic deformations, which exceed the longitudinal minimum by an order of magnitude (see Fig. 5 and Fig.6).

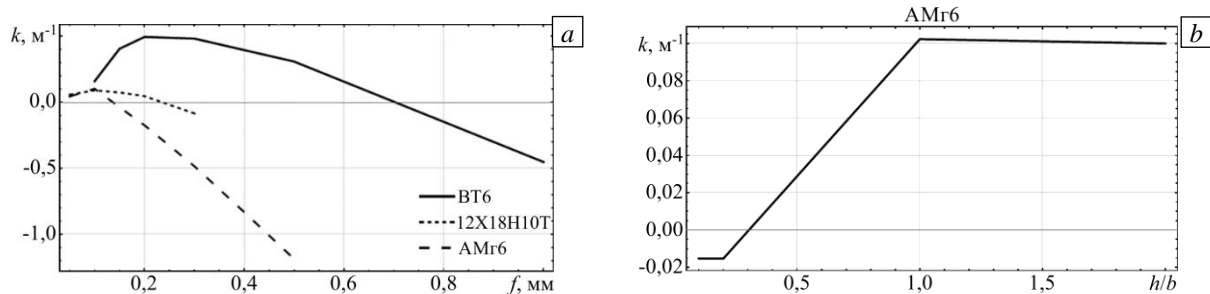


Fig. 7. Dependences of the curvature of square bars made of various materials on the depth of the roller insertion (a); dependence of the curvature of a rectangular beam on its form factor (b).

A more complete picture of the sample distortion is obtained from the analysis of the dependence of the curvature on the dependence of the height to the width of the cross-section (Fig. 7b). Thus, for sample AMg6 rolled to a depth of 0.1 mm, the curve changes its sign sharply with a change in the form factor of the cross-section h/b . Figure 8 shows that this transformation is accompanied by the anticlastic curvature, i.e. a transverse curvature of the sample, which has the opposite sign with respect to the longitudinal curvature. The data in Figure 9 indicate that the distributions of residual stresses and plastic deformations are sensitive to a shape of its sample cross-section. In general, the obtained results indicate the complexity of the problem of controlling the stress-strain state of the samples subjected to surface plastic deformations, even if they have a canonical shape.

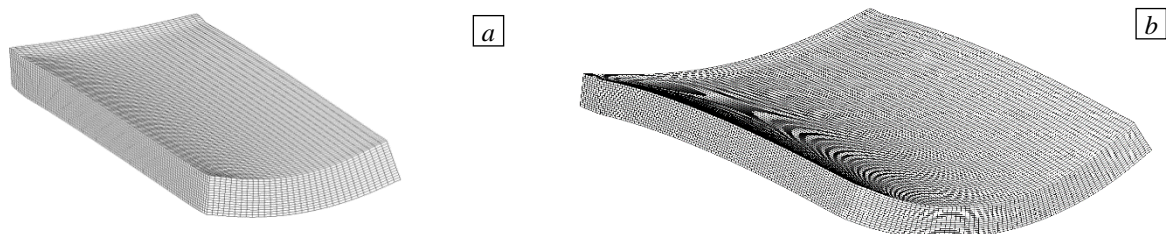


Fig. 8. Anticlastic curvature of AMg6 plates rolled with 0.1 mm roller (the rolling surface is below, displacements are increased by 40 times) at different widths, mm: 50 (a) and 100 (b).

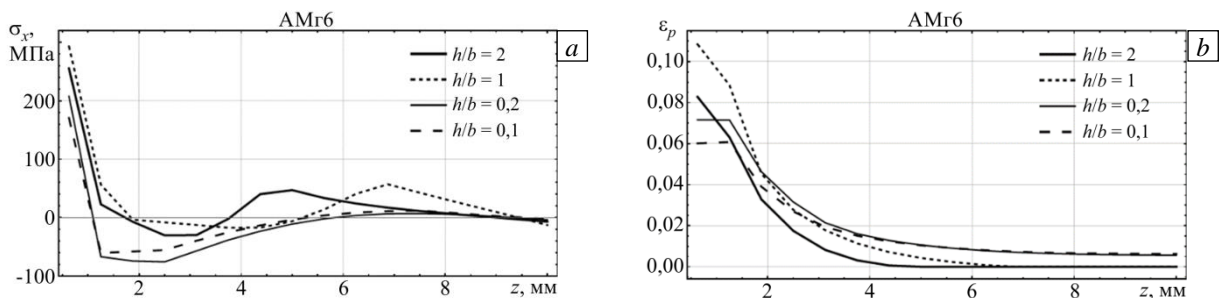


Fig. 9. Distributions of longitudinal residual stresses (a) and accumulated plastic strains (b) over the height of the samples with various form factors of the cross-section.

4. Experimental confirmation of the calculation results

The samples cut from the rolled products AMg6, 12Kh18N10T and VT6 were exposed to the experimental forging with a pneumatic hammer. The samples were subjected to a preliminary heat treatment: aluminum alloy was annealed for 3 hours at 550°C with air cooling; the stainless steel was annealed for 2 hours at 1050°C in an argon atmosphere and cooled together with the furnace; the titanium alloy was quenched for 1 hour at 900°C with air cooling, aging for 3 hours at 500°C and cooling with the furnace. The experiments were carried out using hybrid additive manufacturing facilities designed at the metalworking center. The samples having the rectangular parallelepiped shapes (bars) 240 mm long, 10.3 mm wide, and 23.7 mm high were clamped to a rigid base plate with five screws. By varying the pressure values of the hammer striker to the sample 0.2 and 0.4 MPa and the speed of the striker movement along the sample 150 and 300 mm/min, their optimal values of 0.2 MPa and 300 mm/min were found. It provided a better uniformity of the distribution of plastic deformation along the sample. Figure 2a shows a photo of a forged aluminum alloy sample.

Transverse and longitudinal layers of 2 mm thick were cut from the forged samples using the electroerosive machine (Fig. 2b), the plane-parallel faces of which were machined using R240–R2000 grinding sheets fixed to a lapping plate. The layers served to determine the Vickers microhardness profiles and the tangential components of residual stresses in their plane. The longitudinal layers were cut from the middle of the sample to ensure a uniform distribution of plastic deformations over the thickness.

The HV1 microhardness profiles along the symmetry axis of the layer cut across the sample were found using Shimadzu HMV-G21 microhardness tester with an indentation force of 9.8 N (1 kgf) according to the standard [27]. The distance between the points varied from 20 to 500 μm with a thickening towards the forging surface. The microhardness values shown in Figure 5 demonstrate the presence of a boundary layer near the forging surface, the parameters of which are consistent with the parameters of the boundary layer of plastic deformations.

To use the bending of the sample released from the clamps as an additional parameter to compare the calculation and experimental data, a sample of 240×10×10 mm was made from AMg6 alloy. The forging and clamping surfaces were made flat using the lapping plate. The sample was clamped at the ends and forged within the same parameters as those of the samples described above. The value of the deflection on the base of 200 mm was 1 mm, which differed from the calculated value of 1.21 mm if $f = 0.4$ mm by 21 %.

The profile of residual stresses over the sample thickness was found using an X-ray automatic diffractometer XSTRESS-3000. To do this, in the longitudinal layer along the coordinate corresponding to the sample thickness, with a step of 1 mm, the value of the tangential component of the surface stresses corresponding to the longitudinal coordinate of the sample was obtained. Thus, for a forged beam with a height of 23–24 mm, there were 23–24 values. Neither qualitative nor quantitative agreements with the calculation results could be found in these data. This is probably due to an underestimated role of the transverse components of residual stresses, which are generated by the incompatible part of the inhomogeneous distribution over the cross section of the sample of significant transverse plastic deformations. These components disappear when the longitudinal layer is cut out of the sample.

5. Conclusions

The performed study of the shape distortion of the unloaded sample pre-treated by rolling or forging, as well as the distributions of plastic deformations and residual stresses over its cross-section, makes it possible to specify reliable characteristics that can be used to understand the state of an additively grown linear element after forging. The bending of the unloaded sample is one of such characteristics, which nearly always turns out to be elastic under real forging parameters within this technology, so it can be a measure of longitudinal residual stresses in its unloaded state. Due to inhomogeneity of their distribution over the cross-section of the sample the estimation of residual

stresses entails methodological difficulties. The microhardness profile along the height of the vertical cut of the sample is another characteristic feature. The profile correlates with the distribution of accumulated plastic deformations (work hardening) and makes it possible to understand the depth of plastic deformation localization after the sample has been pressure treated. A nonmonotonic dependence on the running depth of the longitudinal curvature of the beam (and longitudinal residual stresses) is found, which should be taken into account when choosing optimal parameters of the treatment process.

Acknowledgments. The study was supported by Grant from the Russian Science Foundation (Project No. 21-19-00715).

References

1. Colegrove P.A., Coules H.E., Fairman J., Martina F., Kashoob T., Mamash H., Cozzolino L.D. Microstructure and residual stress improvement in wire and arc additively manufactured parts through high-pressure rolling. *J. Mater. Process. Tech.*, 2013, vol. 213, pp. 1782-1791. <https://doi.org/10.1016/j.jmatprotec.2013.04.012>
2. Martina F., Colegrove P.A., Williams S.W., Meyer J. Microstructure of interpass rolled wire + arc additive manufacturing Ti-6Al-4V components. *Metall. Mater. Trans. A*, 2015, vol. 46, pp. 6103-6118. <https://doi.org/10.1007/s11661-015-3172-1>
3. Gu J., Ding J., Williams S.W., Gu H., Bai J., Zhai Y., Ma P. The strengthening effect of inter-layer cold working and post-deposition heat treatment on the additively manufactured Al-6.3Cu alloy. *Mater. Sci. Eng.*, 2016, vol. 651, pp. 18-26. <https://doi.org/10.1016/j.msea.2015.10.101>
4. Gu J., Wang X., Bai J., Ding J., Williams S.W., Zhai Y., Liu K. deformation microstructures and strengthening mechanisms for the wire+arc additively manufactured Al-Mg4.5Mn alloy with inter-layer rolling. *Mater. Sci. Eng.*, 2018, vol. 712, pp. 292-301. <https://doi.org/10.1016/j.msea.2017.11.113>
5. Honnige J.R., Colegrove P.A., Ganguly S., Eimer E., Kabra S., Williams S.W. Control of residual stress and distortion in aluminium wire + arc additive manufacture with rolling. *Addit. Manuf.*, 2018, vol. 22, pp. 775-783. <https://doi.org/10.1016/j.addma.2018.06.015>
6. McAndrew A.R., Rosales M.A., Colegrove P.A., Hönnige J.R., Ho A., Fayolle R., Eytayo K., Stan I., Sukrongpang P., Crochemore A., Pinter Z. Interpass rolling of Ti-6Al-4V wire + arc additively manufactured features for microstructural refinement. *Addit. Manuf.*, 2018, vol. 21, pp. 340-349. <https://doi.org/10.1016/J.ADDMA.2018.03.006>
7. Karunakaran K.P., Kapil S., Negi S. Multi-station multi-axis hybrid layered manufacturing system. Indian Patent. 2018. Application Number 201821038516.
8. Karunakaran K.P., Kapil S., Kulkarni P. In-situ stress relieving process for additive manufacturing. Indian Patent. 2016. Application Number 201621028306.
9. Shchitsyn Yu.D., Krivososova E.A., Trushnikov D.N., Ol'shanskaya T.V., Kartashov M.F., Neulybin S.D. Use of CMT-surfacing for additive formation of titanium alloy workpieces. *Metallurgist*, 2020, vol. 64, pp. 67-74. <https://doi.org/10.1007/s11015-020-00967-0>
10. Shchitsyn Yu.D., Krivososova E.A., Olshanskaya T.V., Neulybin S.D. Structure and properties of aluminium – magnesium – scandium alloy resultant from the application of plasma welding with by-layer deformation hardening. *Tsvetnye Metally*, 2020, no. 2, pp. 89-94. <https://doi.org/10.17580/tsm.2020.02.12>
11. Shchitsyn Yu., Kartashev M., Krivososova E., Olshanskaya T., Trushnikov D. Formation of structure and properties of two-phase Ti-6Al-4V alloy during cold metal transfer additive deposition with interpass forging. *Materials*, 2021, vol. 14, 4415. <https://doi.org/10.3390/ma14164415>
12. Trushnikov D.N., Kartashev M.F., Olshanskaya T.V., Mindibaev M.R., Shchitsyn Yu.D., Saucedo-Zendejo F.R. Improving VT6 titanium-alloy components produced by multilayer surfacing. *Russ. Engin. Res.*, 2021, vol. 41, pp. 848-850. <https://doi.org/10.3103/S1068798X21090264>
13. Horrocks D., Johnson W. On anticlastic curvature with special reference to plastic bending: A literature survey and some experimental investigations. *Int. J. Mech. Sci.*, 1967, vol. 9, pp. 835-861. [https://doi.org/10.1016/0020-7403\(67\)90011-2](https://doi.org/10.1016/0020-7403(67)90011-2)
14. Tan Z., Li W.B., Persson B. On analysis and measurement of residual stresses in the bending of sheet metals. *Int. J. Mech. Sci.*, 1994, vol. 36, pp. 483-491. [https://doi.org/10.1016/0020-7403\(94\)90050-7](https://doi.org/10.1016/0020-7403(94)90050-7)
15. Khiabani A.C., Sadrnejad S.A. Finite element evaluation of residual stresses in thick plates. *Int. J. Mech. Mater. Des.*, 2009, vol. 5, pp. 253-261. <https://doi.org/10.1007/s10999-009-9099-1>

16. Spoorenberg R.C., Snijder H.H., Hoenderkamp J.C.D. Finite element simulations of residual stresses in roller bent wide flange sections. *Journal of Constructional Steel Research*, 2011, vol. 67, pp. 39-50. <https://doi.org/10.1016/j.jcsr.2010.07.004>
17. Essa A., Nasr M.N.A., Ahmed M.H. *Proc. of the 17th Int. AMME Conference. Cairo, Egypt, April 19-21, 2016. P. 37-50.*
18. Kopp R., Schulz J. Flexible sheet forming technology by double-sided simultaneous shot peen forming. *CIRP Annals*, 2002, vol. 51, pp. 195-198. [https://doi.org/10.1016/S0007-8506\(07\)61498-X](https://doi.org/10.1016/S0007-8506(07)61498-X)
19. Petukhov D.S., Keller I.E. Exact reconstruction formulas for plastic strain distribution in the surface-treated plate and their applications. *Acta Mech.*, 2020, vol. 231, pp. 1849-1866. <https://doi.org/10.1007/s00707-020-02625-7>
20. Khan A.S., Huang S. *Continuum theory of plasticity*. John Wiley & Sons, 1995. 421 p.
21. LS-DYNA® Keyword user's manual. Volume II. Material models. Version R11.0. LSTC, 2019. 1613 p. <https://www.lstc.com/download/manuals>
22. Glushak B.L., Ignatova O.N., Pushkov V.A., Novikov S.A., Girin A.S., Sinitsyn V.A. Dynamic deformation of aluminum alloy AMg-6 at normal and higher temperatures. *J. Appl. Mech. Tech. Phy.*, 2000, vol. 41, pp. 1083-1086. <https://doi.org/10.1023/A:1026662824249>
23. Chandrasekaran H., M'Saoubi R., Chazal H. Modelling of material flow stress in chip formation process from orthogonal milling and split Hopkinson bar tests. *Machining Science and Technology*, 2005, vol. 9, pp. 131-145. <https://doi.org/10.1081/MST-200051380>
24. Li L., He N. *Proc. of the Fifth Int. Conf. on High Speed Machining. Metz, France, March 14-16, 2006. P. 759-767.*
25. Maker B.N., Zhu X. Input parameters for springback simulation using LS-DYNA. 6th Int. LS-DYNA Conf. Detroit, USA, April, 2000. 12 p. <https://www.dynalook.com/conferences/international-conf-2000/session12-1.pdf/view> (accessed 10 December 2021)
26. Maker B.N., Zhu X. Input parameters for metal forming simulation using LS-DYNA. 3rd European LS-DYNA Conf. Paris, France, June, 2001. 10 p. <https://www.dynalook.com/conferences/european-conf-2001/58.pdf/view> (accessed 30 October 2021)
27. ASTM E384-17 Standard test method for microindentation hardness of materials. ASTM International, 2017. 40 p.

The authors declare no conflict of interests.

The paper was submitted 01.10.2021; approved after reviewing 10.11.2021; accepted for publication 12.11.2021